Title
Hierarchically nested river landform sequences. Part 2: Bankfull channel morphodynamics governed by valley nesting structure

Authors
Pasternack, Gregory B
Baig, Dastagir
Weber, Matthew D
et al.

Publication Date
2018-05-03

DOI
10.1002/esp.4410

Data Availability
The data associated with this publication are available upon request.

Peer reviewed

Title: Hierarchically nested river landform sequences. Part 2: Bankfull channel morphodynamics governed by valley nesting structure

Short title: Nested river landform sequences, part 2

Authors: Gregory B. Pasternack*, Dastagir Baig, Matthew D. Weber, Rocko A. Brown

University of California, Davis, One Shields Avenue, Davis, CA 95616, USA

* Corresponding author. Tel.: +1 (530) 302-5658

E-mail: gpast@ucdavis.edu

Keywords*:* river topography, river classification, flow convergence routing, fluvial geomorphology

Twitter: The nested structure of flow convergence routing landforms controls bankfull river morphodynamics during moderate to large floods

Cite As: Pasternack, G. B., Baig, D., Webber, M., Brown, R. 2018. Hierarchically nested river landform sequences. Part 2: Bankfull channel morphodynamics governed by valley nesting structure. Earth Surface Processes and Landforms. DOI: 10.1002/esp.4410

Abstract

River corridors exhibit landforms nested within landforms repeatedly down spatial scales. In Pasternack *et al.* (2018), a new, scale-independent, hierarchical river classification was developed that uses five landform types to map the domains of a single fluvial process– flow convergence routing– at each of 3-5 spatial scales. Given those methods, this study investigated the details of how flow convergence routing organizes nested landform sequences. The method involved analyzing landform abundance, sequencing, and hierarchical nesting along the 35-km gravel/cobble lower Yuba River in California. Independent testing of flow convergence routing found that hydraulic patterns at every flow matched the essential predictions from classification, substantiating the process-morphology link. River width and bed elevation sequences exhibit large, nonrandom, and linked oscillations structured to preferentially yield wide bars and constricted pools at base flow and bankfull flow. At a flow of 8.44 times bankfull, there is still an abundance of wide bar and constricted pool landforms, but larger topographic drivers also yield an abundance of nozzle and oversized landforms. The nested structure of flow convergence routing landforms reveals that baseflow and bankfull landforms are nested together within specific floodprone valley landform types, and these landform types control channel morphodynamics during moderate to large floods. As a result, this study calls into question the prevailing theory that the bankfull channel of a gravel/cobble river is controlled by in-channel, bankfull, and/or small flood flows. Such flows may initiate sediment transport, but they are too small to control landform organization in a gravel/cobble river with topographic complexity.

Introduction

Study motivation

For several decades Earth and environmental scientists have conceived of the landscape and its rivers as consisting of hierarchically nested objects (Woldenberg; 1969; Frissell *et al.*, 1986; Hunsaker and Levine, 1995; Imhol *et al.*, 1996; Brierley and Fryirs, 2000; Hay *et al.*, 2001). This conception means the landscape consists of discrete, discernable features that are organized by size, with a small number of larger objects containing an exponentially larger number of smaller objects, repeated down spatial scales until the continuum assumption breaks down (Horton, 1945). Specifically, terrestrial continent objects consist of catchment objects, which in turn consist of subcatchment objects. Subcatchment nesting continues down scales until the scale of hillside and river segment objects (Rodriguez-Iturbe and Rinaldo, 1997). Foregoing hillsides, river segment objects then consist of reach objects, which in turn consist of morphological unit objects, which in turn consist of hydraulic unit objects, which in turn consistent of surficial roughness objects (Thomson *et al*., 2001).

Object-based hierarchical conceptualization allowed for the development of independent questions, methods, and results at each scale (Pasternack, 2011) as well as corresponding management solutions (Beechie *et al.*, 2010). The dominant scientific paradigm of empirical, field-based research at each scale involved representative sampling with a very small number of samples, because research was data-limited (Brennan *et al.*, 2002; Smith and Jones, 2008). In some cases, tests were done to ensure that results were not impacted by insufficient sampling (e.g., Angermeier and Smogor, 1995). Such testing has yielded mixed results, especially for physical studies (e.g., Thomson *et al.*, 2004; Gonzalez and Pasternack, 2015). Most often, no such testing was possible in the absence of a population census to test against. Many scientific ideas and practical applications therefore make assumptions about spatial scaling that are largely untested. As a result of the lack of commensurate data and results, it is extremely difficult to synthesize a universal scientific conceptualization based on empirical research that works across all scales.

In contrast to the object-oriented hierarchical nesting paradigm of data-limited settings, data-rich systems are predominantly analyzed using signal processing methodologies (Priestley, 1981) that deconstruct data series in time or space (or both) to find patterns at each scale (Pawlowicz*et al.*, 2002) and ones that transcend scales (Barenblatt and Monin, 1979; Rodriguez-Iturbe and Rinaldo, 1997). These analyses use the finest resolution data support. They have unified questions, methods, and results that work across all scales to provide a coherent, universal conceptualization. For Earth's surface data, this approach has been feasible using remotely sensed raster data (Kumar and Foufoula-Georgiou, 1997; Jakubauskas *et al.*, 2002), but pixel resolution has been too coarse (~ 30-100 m) for fluvial geomorphology. Topographic data at that scale has poor vertical accuracy (Neeson *et al.*, 2008).

Mapping of the Earth's surface can now achieve a near census (1-m) sampling of the population of elevation (Westoby et al., 2012), LiDAR intensity (Mandlburger *et al.*, 2015), and electromagnetic multi-spectral properties (Legleiter *et al.*, 2009). There remain finer levels of continuum detail that ground-based technology addresses over small areas (Brasington *et al*., 2012), and will eventually span at the landscape scale. Nevertheless, the 1-m, near-census scale of data acquisition is capable of fundamentally transforming analysis of hierarchically nested landscapes. Studies pursuing this for science (Legleiter, 2014; Pasternack and Wyrick 2016; Brown and Pasternack, 2017) and management (Brown *et al*., 2014; Pasternack and Brown, 2016) are emerging.

Study purpose

The overall goal of this study was to reenvision the notion of hierarchical nesting in rivers and reveal a new understanding of river patterning. Prior to this study, object-oriented river classifications used unique typologies at each scale that are incommensurate with those at other scales (see citations in first sentence of this article). In Pasternack *et al.* (2018), we proposed a new, continuum-based, scale-independent approach to classifying landforms with respect to a single morphodynamic mechanism that can occur at many fluvial scales. The approach is amenable to signal processing analyses that enable the same typology to be employed over the same wide range of scales that the mechanism spans. This capability provides a unified theory of fluvial process-morphology linkages for any one process. We chose the mechanism of flow convergence routing as the illustrative mechanism to focus on (see Pasternack *et al.* (2018) for background literature, classification scheme, and data analysis methods).

In this article, we apply the classification and analysis framework to spatial series of topographic data from a 35-km gravel/cobble bed river corridor to reveal the abundance, sequencing, and nesting of scale-independent landforms relevant for understand flow convergence routing. There are four study objectives- three to analyze the landforms and one to validate the velocity pattern assumed by the underlying classification theory. For each objective, there are three to five specific, tractable questions (Table 1). Some results from this application support existing concepts about fluvial geomorphology, while others present significant evidence against prevailing wisdom; hence this article is not merely descriptive but tests fundamental scientific ideas about rivers.

Study area

Geographic Setting

The Yuba catchment in California drains 3480 km^2 of Dry Summer Subtropical mountains down to the confluence with the Feather River (Figure 1). Like many mountain catchments, this one experienced anthropogenic impacts, notably hydraulic gold mining (Gilbert, 1917), timber harvesting, and flow regulation. Englebright Dam was built in 1940 to trap nearly all sediment and thereby promote downstream geomorphic recovery, which continues to proceed more than 70 years later (Carley *et al.*, 2012). Daguerre Point Dam (DPD) is an 8-m high irrigation diversion structure located at river kilometre (RKM) 17.8 that creates a slope break and partial sediment barrier.

The 37.1-km LYR segment (Figure 1) is a single-thread channel (~ 20 emergent bars/islands at bankfull) with low sinuosity, high width-to-depth ratio, slight to no entrenchment, and eight distinct geomorphic reaches (Wyrick and Pasternack, 2012). The river segment has a mean bed slope of 0.185% and a mean surface substrate diameter of 97 mm (i.e., small cobble). As a comparison to other rivers, the LYR is classified as a C3 channel by the Rosgen (1994) Stream Type classification method when applied to the segment and as transitional straight-meandering by the flow instability method. This study investigated the six alluvial geomorphic reaches as one segment and by reach (Figure 1).

The LYR corridor has natural canyon and valley walls in the first 9 RKM below Englebright Dam, and there are major artificial constraints on corridor width. The river corridor is confined in a steep-walled bedrock canyon for the upper 3.1 RKM, then transitions first into a wider bedrock valley with some meandering through Timbuctoo Bend (RKM 28.3-34.0), then into a wide, alluvial valley downstream to the mouth. During the late 19th to mid 20th century, gravel and gold miners dredged and re-arranged the topography of the LYR creating high and wide berms of dredger mine tailings that isolate the modern river from the ~ 40-km^2 of extremely disturbed landscape (Yuba Goldfields), which is still actively mined. Upstream of the Yuba Goldfields there are two major artificial mine-tailing berms within Timbuctoo Bend. Downstream of the Yuba Goldfields river corridor width is constrained by agricultural land use and engineered levees. All of these forced geographic controls on width and width undulation drive geomorphic responses in bed elevation and its downstream undulation in turn (Brown and Pasternack, 2014, 2017). Such links are further investigated in this study.

Hydrogeomorphic Regime

This study investigates landform patterns associated with flows spanning 0.14 to 8.44 times bankfull discharge (Q_{bf}), which equals 19.82 to 1195 m^3/s. Regulated LYR base flows are commonly between ~ 14 and 23 m^3/s, with a flow of 19.82 m^3/s serving as the negotiated minimum release from Englebright Dam during all but the driest years. Different locations along the river exhibit spillage out of the channel into low-lying peripheral swales and onto lateral and point bars at flows from ~ 84.95 to 141.6 m^3/s. When water stage rises to 141.6 m^3/s, relatively flat active bar tops become inundated and the wetted extents line up with the base of willows along steeper banks flanking the channel. Based on these and other field indicators, 141.6 m^3/s represents Q_{bf} adjusted to the modern regulated flow regime since 1970. This flow has ~ 82% annual exceedence probability. By a flow of 198.2 m^3/s, banks are all submerged and water is spilling out to various degrees onto the floodplain. The modern floodplain is considered fully inundated when the discharge reaches 597.5 m^3/s, so this is the water surface area referred to herein as the "floodway". Above this flow, alluvial terraces, bedrock outcrops, training berms, and soil-mantled hillsides become inundated. A flow of 1195 m^3/s yields a depth twice that of bankfull discharge (Wyrick and Pasternack, 2012), which by definition fills the floodprone area, as defined by Rosgen (1994).

Methods

Data used in this study consisted of a DEM, geomorphic reach breaks, water surface area polygons, and depth-average velocity rasters earned through years of fieldwork, quality assurance procedures, and mechanistic numerical modeling. They were thoroughly vetted and published in peer reviewed technical reports and journal articles.

River corridor topography and bathymetry were collected for the meter-resolution DEM using a combination of airborne LiDAR, ground-based surveying, and boat-based sonar. Each method involved its own internal performance tests and yielded different point densities (complete details in Pasternack *et al.*, 2014; Strom *et al.*, 2016). For example, within and beyond the 24.92 m^3/s water surface area, point density downstream of TBR was 59 and 554 pts/100 m^2, respectively.

Water surface area polygons from a published meter-scale 2D hydrodynamic model (solved with the United States Bureau of Reclamation SRH-2D algorithm) were available for 28 flows ranging from 8.50 to 3126 m^3/s (Abu-Aly *et al.*, 2013; Pasternack *et al.*, 2014). This study focused on evaluating spatial series of detrended, standardized, cross-sectionally averaged bed elevation (Zs), standardized cross-sectional top width (Ws), Ws·Zs, and landforms identification codes at five representative flows– 19.82, 141.6, 283.2, 597.5, and 1195 m^3/s– whose significance was explained in the study area section, except 283.2 m^3/s, which is simply $2 \cdot Q_{bf}$. In addition to the five flows previously listed, velocity data for four other flows (17.63, 28.32, 2390, and 3126 m^3/s) were used to improve the detail of the velocity-discharge hydraulic geometry relation and span larger floods when addressing objective two. For objective four, landform nesting was investigated at three scales, the perennial base flow channel ($0.14 \cdot Q_{bf}$), the bankfull channel (Q_{bf}), and the floodprone valley floor ($8.44 \cdot Q_{bf}$).

The bisecting centerline of the water surface area at each flow was obtained using ArcGIS® version 10.3. Centerlines were stationed with a spacing of 3% of mean bankfull channel width. In this study, the bankfull width was ~ 100 m (Wyrick and Pasternack, 2012) and spacing had to be done in American customary units (10 ft), so in metric units the spacing was 3.048 m.

Pasternack (2011) provided workflows for obtaining water surface area polygons and velocity magnitude rasters from SRH-2D outputs. Many 2D model validation tests were done for an order of magnitude range of flow from ~ 14 to 170 m^3/s (Barker, 2011). Water surface elevation, depth, velocity magnitude, and velocity direction model performance was on par or better than accepted scientific norms. Median unsigned velocity magnitude error was 16%, which is less than commonly reported.

Data analysis methods (Table 1) were explained in Pasternack et al. (2018). Each analysis was implemented using ArcGIS® 10.3 for geospatial processing and Microsoft Excel® for statistical analysis. Analyses by discharge were performed on each geomorphic reach and the whole river segment to compare and contrast reach-dependent hierarchical controls on landform organization.

Results

Structure of topographic heterogeneity

Every analysis performed in this study provided a strong corroboration building on the previous study of TBR by Brown and Pasternack (2017). Specifically, the LYR is

Table 1. Scientific analysis framework for this study applied to whole river segment and each geomorphic reach.

Objectives (O#) and their questions	Test variables	Analysis
(O1) Analyze stage-dependent structure of fluvial topographic deviation from central tendency using longitudinal series of standardized width (Ws) and detrended, standardized bed elevation (Zs)		
(1a) What percent of the river has topographic variations greater than 0.5 and one standard deviations away from the mean?	Abs(Zs), Abs(Ws)	percent of values > 1
(1b) Is longitudinal topographic structure random?	series of Zs, Ws	Wald-Wolfowitz runs tests
(1c) Are width and bed elevation series correlated, as one indicator of coherent organization?	series of Zs, Ws	Pearson's product-moment correlation for Ws and Zs
(1d) Is the specific longitudinal structure of the river's morphology consistent with a dominant role for flow convergence routing?	series of Ws·Zs	mean(Ws·Zs); percent of values > 0
(O2) Do landforms classified in this system exhibit the specific stage-dependent differences in velocity (V) expected by the flow convergence routing mechanism?		
(2a) Does oversized have lower velocity than normal channel and does the latter have lower velocity than nozzle?	0.91-m V raster from 2D hydrodynamic model	mean(V) and V95* among raster cells in landform
(2b) Are constricted pool landforms low velocity at base flow and high velocity at flood flow?	0.91-m V raster from 2D hydrodynamic model	mean(V) and V95* among raster cells in landform
(2c) Are wide bar landforms high velocity at base flow and low velocity at flood flow?	0.91-m V raster from 2D hydrodynamic model	mean(V) and V95* among raster cells in landform
(O3) Analyze relative abundance and longitudinal sequencing of landforms by reach and discharge.		
(3a) What is the relative abundance of each landform for the whole river for each flow?	series of landform IDs	count and compare
(3b) How do geomorphic reaches compare in landform composition?	series of landform IDs	count and compare
(3c) How does landform abundance change with flow?	series of landform IDs	count and compare
(3d) What is the longitudinal sequencing of landforms?	series of landform IDs	count times each unit followed another
(3e) How does longitudinal sequencing change with flow?	series of landform IDs	count times each unit followed another
(O4) what is the stage-dependent, nested structure of landforms classified by their flow convergence routing potential?		
(4a) What are top five most abundant nested permutations?	nested series of landform IDs	permutation abundance analysis
(4b) For each landform at the floodprone scale, what are the top five most abundance nested permutations?	nested series of landform IDs	permutation abundance analysis
(4c) For each landform at the bankfull scale, what are the top five most abundant nested permutations?	nested series of landform IDs	permutation abundance analysis
(4d) For each landform at the bankfull scale, what are the top three most abundant floodprone landform hosts?	nested series of landform IDs	permutation abundance analysis

*V95 is the 95th percentile value of velocity among all 0.91-m pixels in the area of any one landform type primarily defined by its variability, not its central tendency. Stations along the river rarely exhibited Zs or Ws values of zero, and instead exhibited wide swings (Figure 2). The Wald-Wolfowitz runs test showed that Zs and Ws series were nonrandom at all flows tested ($p<10^{-6}$).

At nearly all flows, more than half the river's bed length had Zs values > 0.5 standard deviations away from the mean value, and almost two-thirds of it had Ws values beyond that criterion (Table 2). Approximately a quarter of the river's bed length had Zs and Ws values more than one standard deviation high and low. MR and TBR had the most extreme bed undulations, while DPDR and DCR had the most uniform beds (Figure 2).

Because width was standardized at the segment scale, the mean Ws for each reach (Table 2c) was free to deviate from the overall central tendency. Some reaches (DCR and DPDR) were especially wide, while others were especially narrow (MR and TBR). The two reaches with the most uniform Zs (DPDR and DCR) were also the widest on average. DCR was wider than average at all flows and was widest at 1-2 times Q_{bf}, whereas DPDR was an average width for in-channel flows, but abruptly widened a lot after $2 \cdot Q_{bf}$ (Figure 3). Greater widths are explained by the presence of a secondary anastomosing channel and excellent floodplain connectivity in that reach.

Moving from reach-average width to Ws variability, MR was not only narrow with extreme Zs variations, but it also had the most extreme Ws variations (Table 2d,e). PBR had a normal abundance of extreme widths for in-channel flows, but its overbank flows were unusually constricted. This result is explained by the presence of historically created artificial terraces of dredged coarse sediment. DCR showed a similarly

Table 2. Metrics for topographic variability. Dark and light shading indicate high and low values, respectively.

flow (xQbf)*	Segment	Geomorphic reaches** MR	HR	DPDR	DCR	PBR	TBR
A) % Abs(Zs)>0.5							
0.14	59	67	57	41	52	60	72
1	58	69	58	36	39	61	75
2	57	70	60	35	30	59	75
4.22	53	73	63	36	16	45	67
8.44	47	87	21	34	25	58	58
(B) % Abs(Zs)>1							
0.14	29	36	20	10	23	30	50
1	28	38	25	5	15	29	49
2	28	52	26	5	8	25	47
4.22	25	54	25	7	5	15	39
8.44	21	70	3	5	6	19	31
(C) Ws mean							
0.14	0.00	-0.03	-0.09	-0.17	0.49	-0.15	0.16
1	0.00	-0.63	0.20	0.14	0.80	0.00	-0.34
2	0.00	-0.81	0.26	0.29	0.94	0.00	-0.50
4.22	0.00	-0.97	0.12	1.29	0.52	-0.01	-0.74
8.44	0.00	-0.84	0.01	1.28	0.32	0.18	-0.82
(D) % Abs(Ws)>0.5							
0.14	62	65	54	63	66	66	63
1	63	81	68	43	64	63	60
2	66	86	70	49	70	60	65
4.22	69	85	73	94	58	40	70
8.44	65	82	61	94	26	44	81
(E) % Abs(Ws)>1							
0.14	28	27	17	25	38	34	33
1	29	37	35	15	39	28	24
2	32	57	44	16	48	14	20
4.22	39	71	37	75	14	11	35
8.44	40	61	38	74	21	15	36

*Flow values are given in multiples of bankfull discharge

**Reach names as given in Figure 1.

significant decline in width variability with flow, but that did not happen until after $2 \cdot Q_{bf}$. DPDR showed a significant increase in extreme widths above $2 \cdot Q_{bf}$.

For in-channel flows, although the abundance of Ws extremes was equal to that of Zs extremes, the higher flow rose above bankfull, the more Ws deviated from its central tendency (Table 2d,e; Figure 3). The segment as a whole secularly decreased its Zs variability and secularly increased its Ws variability with increasing discharge, but no reach does either on its own. MR was the only reach that increased its Zs and Ws variability with discharge.

Given that Zs and Ws showed significant, nonrandom variations along the LYR at all flows tested, the next analysis tested whether those were linked. The landform classification developed in this study does not need them to be, but the interpretation of flow-dependent hydrogeomorphic processes depends on how they relate. All Pearson's product-moment correlation coefficient (r) values were positive correlations statistically significant at the 99% confidence level (Figure 4). That means that when a water surface area is narrow (low Ws), it tends to be deep (low Zs); when it is wide (high Ws), it tends to be shallow (high Zs). That result is consistent with an interpretation that the river is primarily organized into constricted pools, normal channels, and wide bars. Eleven out of 35 cases (31%) had a r-value > 0.7, which means Zs and Ws variations were directly linked to a significant degree. No reach always had the highest r-value across all flows, but HR and TBR had the highest average of r-values among flows, while DCR had the lowest. Among flows, the highest r-value for the river segment existed for Q_{bf}, with a close second by $2 \cdot Q_{bf}$. Meanwhile, the highest and lowest flows had the lowest and second lowest r-values, respectively.

The last test pushed further to aid interpretation of flow convergence routing by assessing the sign and magnitude of Ws·Zs, also known as the "geomorphic covariance" (Brown and Pasternack, 2014, 2017). The mean value of Ws·Zs was above zero for all flows (Table 3a) and the series of Ws·Zs consisted of both ++ and -- combinations, indicating a predominance of self-sustainable constricted pool and wide bar units, capable of rejuvenating themselves by way of the flow convergence routing mechanism. Further, the vast majority of Ws·Zs values were positive for all flows (Figure 5). Most interestingly, Q_{bf} had the highest mean Ws·Zs value and the highest percent of station Ws·Zs values above zero (Table 3b). The lowest mean and percent positive Ws·Zs values occurred for the largest flood investigated (Figure 5). All reaches, except MR and HR exhibited a decrease in Ws·Zs above Q_{bf}. HR also exhibited a decrease in Ws·Zs, but it did not begin until after $2{\cdot}Q_{bf}$. MR had a unique large increase in mean Ws·Zs with discharge, which is consistent with its narrowing and increased bed and width undulations with discharge. Finally, correlation between the Ws·Zs values for a given flow and the sequentially higher flows went down as discharge increased, with the highest correlation for Q_{bf} versus $2{\cdot}Q_{bf}$, similar to results from Brown and Pasternack (2017).

Landform-stratified velocity

Landform classification was applied to the Ws·Zs longitudinal series (colors in Figure 5). Prior to analyzing those results, 2D model velocity rasters were tested for the expected relative differences in velocity among landform types required of the flow

Table 3. Results of Ws·Zs analysis. Dark and light shading indicate highest and lowest values, respectively.

flow (xQbf)	Segment	MR	HR	DPDR	DCR	PBR	TBR
(A) mean Ws·Zs							
0.14	0.46	0.26	0.40	0.33	0.48	0.51	0.76
1	0.62	0.59	0.77	0.31	0.45	0.67	0.78
2	0.55	0.66	0.80	0.26	0.24	0.51	0.65
4.22	0.40	0.92	0.56	0.07	0.09	0.29	0.35
8.44	0.32	1.24	0.17	0.12	0.20	0.15	0.24
(B) percent of Ws·Zs >0							
0.14	70	61	75	74	71	73	64
1	77	63	86	82	65	84	72
2	77	65	86	77	63	89	67
4.22	66	73	76	48	65	77	49
8.44	62	74	60	57	68	70	46

convergence routing morphodynamic mechanism. The results largely matched expectations, corroborating the theoretical underpinnings of this framework. Both landform-averaged velocity and the 95th percentile of raster cell velocities in each landform show the same relationships (Figure 6). For all discharges, oversized had lower mean velocity and 95th percentile of velocity than normal channel, which in turn had lower values than nozzle. The values were most differentiated for the lowest and highest discharges tested and closest at $2 \cdot Q_{bf}$. Meanwhile, constricted pool and wide bar showed the expected velocity divergence, with the former having a steep rate of increase in velocity with increasing discharge and the latter having a gentle one (Figure 6). At the lowest discharge, constricted pool velocity was lower than wide bar velocity for both velocity metrics. The velocity reversal between these two landforms occurred between the lowest and second lowest discharges, but constricted pool had a relatively high velocity even at low discharge. Beginning at Q_{bf} and for all higher flows, constricted pool had significantly higher velocity than wide bar for both metrics. In essence, normal channel, constricted pool, and wide bar all had similar cross-sectional areas at low flows, so they had similar velocities. For overbank flows, their cross-sectional areas dramatically diverged, causing the associated change in flow convergence routing.

The most interesting velocity results came from comparing wide bar versus oversized and constricted pool versus nozzle. Velocity reversals occurred in which nozzle and oversized had the most extreme velocities for in-channel flow, but for overbank flows constricted pool and wide bar had them at some flows (Figure 6). These results are consistent with the theoretical expectation that constricted pools exhibit flow convergence routing during floods, while wide bars have low velocities and thus may receive the sediment scoured out of pools.

Yet it is also evident that the decision tree is not yielding the purest theoretical outcome wherein nozzle should universally have the highest velocity and oversized the lowest. Three sample velocity maps illustrate why this outcome is occurring (Figure 7). The maps are briefly described as results, and then a mechanistic explanation is provided in the discussion section. For in-channel flows, 2D model hydraulics closely conform with the expectations of the landform classification, with longitudinal variation in velocity dominating over lateral variation. For example, nozzles are the fastest and oversized slowest (Figure 7a). However, during flood flows, the flow field exhibits strong lateral gradients that can match or confound expectations. For example, at one MR site the constricted pool definitely has a uniformly high velocity for the majority of its width, and the constricted pool's velocity is higher than that in the upstream wide bar (Figure 7b). However, the wide bar has a strong lateral gradient with a core of high velocity in the bankfull channel and a range of lower velocities across the whole inundated bar complex. Thus, on average the wide bar is lower velocity than the constricted pool and its 95th percentile of velocity is lower than that of the constricted pool, conforming to flow convergence routing theory, even if the average state does not convey the whole story of the hydraulic mechanism at play.

However, the situation at the highest flows is where the complexity of natural 2D flow fields defies the purest form of a cross-sectionally averaged interpretation of flow convergence routing. For example, during the floodprone flow of 8.44·Qbf, constricted pool again showed a large fraction of its cross-sectional areas as having very high velocity, whereas the nozzle upstream of it was comparatively wider (though still narrow compared to segment-wide flow width) and had a slower central velocity core surrounded by a wide area of low velocity (Figure 7c). This velocity pattern is a classic example of a modest effective flow width. Thus, constricted pool had a higher effective flow width and higher cross-sectional velocity than nozzle, which is explained in the discussion section.

Landform abundance and sequencing

Even though much of the LYR exhibited a positive correlation between Ws and Zs, there were locations with a negative correlation, yielding a diversity of landforms when viewed from the lens of flow convergence routing. Among all flows and considering the whole segment, normal channel was the most abundant morphology and oversized was the least abundant (Table 4; Figure 5). Further, wide bar and constricted pool were present in a similar medium abundance, with slightly more constricted pool. Oversized and nozzle were in a similar low abundance, with slightly more nozzle. At the segment scale, there was no trend in the composition of morphologies as flow increased. The second highest flow was different, with more of all types at the expense of normal channel, but at the highest flow the typical composition had returned.

Considering differences between reaches that were common among all flows, DPDR and DCR, which had the most uniform bed elevations, also had the most length of normal channel (Table 4). MR and TBR, which had the most undulating bed elevations, had the least normal channel. MR (the narrowest) had the most nozzle and constricted

Table 4. Analysis of landform composition as a function of flow.

flow (xQbf)	% of XS locations				
	O*	CP*	NC*	WB*	NZ*
(A) segment					
0.14	2.2	16	61	16	4.7
1	0.6	21	58	18	3.4
2	0.8	21	58	17	3.6
4.22	8.3	25	36	20	9.7
8.44	3.7	16	62	11	6.3
(B) MR					
0.14	5.4	13	55	14	12
1	0.00	34	42	7	16
2	0.00	38	33	8	20
4.22	0.00	55	13	10	22
8.44	0.8	46	20	17	16
(C) HR					
0.14	0.2	16	69	14	0.5
1	0.3	21	55	24	0.04
2	0.5	20	54	25	0.5
4.22	8.6	27	29	32	3.0
8.44	0.00	13	74	9.0	4.8
(D) DPDR					
0.14	0.1	14	74	10	1.9
1	0.3	7.6	79	13	0.0
2	0.6	8.0	78	13	0.1
4.22	36.0	0.0	26	38	0.0
8.44	16.1	0.1	59	25	0.0

*O=oversized, CP=constricted pool, NC=normal channel, WB=wide bar, NZ=nozzle

flow (xQbf)	% of XS locations				
	O*	CP*	NC*	WB*	NZ*
(E) DCR					
0.14	1.7	17	60	20	1.9
1	4.2	8.0	66	21	0.0
2	5.3	4.3	69	22	0.0
4.22	8.6	5.6	67	19	0.0
8.44	1.4	0.0	85	13	0.0
(F) PBR					
0.14	1.1	21	55	18	5.2
1	0.4	21	56	23	0.0
2	0.3	20	62	17	0.0
4.22	1.1	22	58	19	0.4
8.44	5.4	12	74	8.0	0.3
(G) TBR					
0.14	5.9	17	49	21	7.5
1	0.00	27	54	13	6.4
2	0.00	30	55	11	4.2
4.22	0.00	37	28	1.9	33
8.44	0.00	24	58	1.2	16

pool. Wide bar was relatively abundant in all reaches, except MR and TBR. DPDR had the most oversized channel.

Differences between reaches were also present as a function of discharge (Table 4). MR and TBR showed a decrease in normal channel as discharge increased, and this was offset by an increase in constricted pool. TBR also showed a significant decrease in wide bar offset by an increase in nozzle, with a significant increase in nozzle above $2 \cdot Q_{bf}$. This result shows the effect of artificial mine-tailing berms and natural valley hillsides in TBR activating as firm constrictions. HR showed a significant increase in wide bar from $0.14 \cdot Q_{bf}$ to $4.22 \cdot Q_{bf}$, but then at the highest flood, wide bars became normal channel. DPDR exhibited a unique flow dependence in which oversized and wide bar became significantly more abundant after $2 \cdot Q_{bf}$, which was explained by the presence of a secondary anastomosing channel to the north of its perennially inundated main channel. DCR had a typical abundance of constricted pool at base flow, but that declined with discharge and went to zero for the largest flood. PBR was the most uniform in its composition as discharge increased.

Beyond landform composition, landform sequencing was also analyzed to understand how flow convergence routing was structured in the river. In theory, an ideal river with flow convergence routing at any scale would have a sequence that alternates between wide bar and constricted pool, which would necessitate some length of normal channel in between to make the transition. However, this ideal was not expected, because most rivers have forcing elements that also induce nozzles and oversized unit, so the question involved ascertaining whether the percentage of transitions between wide bar and constricted pool were higher than would occur by random chance alone.

Across all flows, all units predominantly transitioned to normal channel, because any time there is a zero-crossing for Ws·Zs, then that means the presence of normal channel. Though it was plausible that a wide bar might follow a constricted pool (and vice versa) or that a nozzle might follow an oversized channel (and vice versa), the results showed that this almost never happened– at least not with the highly conservative thresholds for normal channel used in this study.

When normal channel was excluded from sequencing analysis, then the results supported the presence and importance of flow convergence routing in maintaining landform differentiation. The number of times that constricted pool was followed by wide bar, or vice versa, was highest for Q_{bf} and $2 \cdot Q_{bf}$, but then decreased as flow went up or down from those flows (Table 5). The percents at Q_{bf} (55 and 69%) were significantly higher than expected at random given three possible transitions (33%), which is a strong indicator of preference. Conversely, they were significantly lower at the two largest floods tested (9 and 19%), which is a strong indicator of avoidance. At all flows, oversized channel was predominantly followed by wide bar, while nozzle was predominantly followed by constricted pool. This sequencing reflects the geometric condition that when a reach is universally narrow at a given flow, then its sub-reach-scale landforms alternate between nozzle and constricted pool. Conversely, when a reach is universally wide at a given flow, then its sub-reach-scale landforms alternate between oversized and wide bar. This discharge-dependent result was especially dominant at the two highest floods tested; it is the first indication of hierarchical nesting in the study– narrow large landforms tend to have narrow small landforms nested in them, while wide large landforms tend to have wide small landforms nested in them.

Table 5. Longitudinal sequencing of landforms for the whole river, excluding normal channel units. Shading indicates highest values.

	% of times unit followed starting unit			
Starting unit	O*	CP*	WB*	NZ*
(A) 0.14·Qbf				
O	--	33	67	0
CP	31	--	43	26
WB	15	45	--	39
NZ	5	64	32	--
(B) Qbf				
O	--	30	70	0
CP	0	--	69	31
WB	32	55	--	12.9
NZ	0	85	15	--
(C) 2·Qbf				
O	--	15	85	0
CP	6	--	66	28
WB	31	57	--	11
NZ	0	77	23	--
(D) 4.22·Qbf				
O	--	13.3	87	0
CP	5	--	19	76
WB	67	10	--	24
NZ	0	81	19	--
(E) 8.44·Qbf				
O	--	17	83	0
CP	12.1	--	9	79
WB	67	19	--	14
NZ	0	90	10	--

*O=oversized, CP=constricted pool, WB=wide bar, NZ=nozzle

Further, given that Zs cannot control floodprone width in reaches with artificial or strong natural constrictions, then it also shows that Zs is more of a response variable than Ws.

Landform nesting

Eighty-five permutations of the 125 nesting possibilities had at least one occurrence, while the remaining 40 had no occurrence. The most common permutation by far was the strictly defined normal channel across all flows, which occurred for 16% of stations. Thus, while most abundant, it was still not particularly common. The next four most common permutations were normal channel at $0.14 \cdot Q_{bf}$ and Q_{bf} nested within a wide bar at $8.44 \cdot Q_{bf}$, the same nested within a constricted pool at $8.44 \cdot Q_{bf}$, the same nested within oversized channel at $8.44 \cdot Q_{bf}$, and wide bar at $0.14 \cdot Q_{bf}$ and Q_{bf} nested within normal channel at $8.44 \cdot Q_{bf}$. These results show that nesting permutation frequencies mimic landform abundance; because normal channel is the most abundant landform at all flows (Figure 5), then there is simply a higher probably of its nesting permutations also being most abundant. This result is further revealed by looking at the top five permutations of base flow and bankfull flow landforms within each of the five floodprone landform types (Table 6). The presence of normal channel participating in nesting with another unit was the top permutation in each case, and several of the other top permutations involve normal channel at some level.

It is usually possible to handle the problem of widely different landform abundances by normalizing an analysis by abundance (e.g., Wyrick and Pasternack, 2014), but in the case of permutation analysis that is not possible. Instead, the question was posed in

Table 6. Top five permutations of hierarchical nesting of flow convergence routing landforms within the five floodprone landform types.

Landform ID*				
8.44·Qbf	Qbf	0.14·Qbf	count	% of river
(A) Nested within floodprone nozzle				
NZ	NC	NC	379	3.2
NZ	CP	NC	213	1.8
NZ	CP	CP	125	1.1
NZ	NC	WB	123	1.0
NZ	WB	WB	118	1.0
(B) Nested within floodprone wide bar				
WB	NC	NC	1010	8.6
WB	NC	CP	173	1.5
WB	WB	NC	165	1.4
WB	NC	WB	156	1.3
WB	CP	NC	154	1.3
(C) Nested within floodprone normal channel				
NC	NC	NC	1924	16
NC	WB	WB	481	4.1
NC	NC	WB	438	3.7
NC	WB	NC	424	3.6
NC	CP	NC	422	3.6
(D) Nested within floodprone constricted pool				
CP	NC	NC	845	7.2
CP	CP	NC	480	4.1
CP	CP	CP	284	2.4
CP	NC	WB	201	1.7
CP	NC	CP	109	0.9
(E) Nested within floodprone oversized				
O	NC	NC	592	5.0
O	WB	NC	169	1.4
O	NC	CP	146	1.2
O	NC	WB	83	0.7
O	CP	CP	73	0.6

*O=oversized, CP=constricted pool, NC=normal channel, WB=wide bar, NZ=nozzle a different way, which was to ask what the other bankfull landforms are nested in and what is nested within them? This time, the top three permutations were tallied.

Because classic velocity reversal theory anticipates a two-stage flow convergence routing mechanism, then the expectation is that wide bar and nozzle landforms acting as riffles at base flow should be nested within wide bar bankfull landforms. Further, oversized and constricted pool base flow landforms should be nested within constricted pool bankfull landforms. This expectation was largely met (Table 7a-e; Figures 5 and 8). In fact, in each case, the situation in which the same landform type was nested within itself occurred within the top 2 out of 5 possible permutations every time. Further, wide bar had nozzle nested in it and constricted pool had oversized within it, meeting expectations. Bankfull wide bar did not have oversized or constricted pool base flow landforms preferentially nested in them, nor did bankfull constricted pool have wide bar or nozzle preferentially nested. Figure 9a,b illustrate a ~ 2.5-km section of the river in which four out of five base flow nozzles are nested within bankfull wide bars.

Considering bankfull nesting, bankfull nozzles exhibited nozzles and wide bars nested in them, which affects the interpretation significantly. If the base flow channel were set by topographic steering at bankfull flow per classic theory, then one would expect to see scoured, deep (negative Zs) units nested within bankfull nozzle, assuming the bed material is equally erodible in all unit types. The reason is that by definition and as affirmed in the velocity results in this study, nozzle has a high sediment transport capacity and thus should promote scour of the things inside of it. Using more traditional terminology, the expected pattern would be to have a bankfull riffle with one or more constricted base flow chutes nested within. Instead, bankfull nozzles had shallow

Table 7. Top three permutations of hierarchical nesting of bankfull landforms, either within (A-E) or beyond (F-J) them.

Qbf	0.14·Qbf	count	% of river	8.44·Qbf	Qbf	count	% of river
(A) within bankfull nozzle				(F) hosting bankfull nozzle			
NZ	NZ	228	1.9	NC	NZ	139	1.2
NZ	NC	152	1.3	NZ	NZ	132	1.1
NZ	WB	46	0.4	WB	NZ	103	0.9
(B) within bankfull wide bar				(G) hosting bankfull wide bar			
WB	NC	864	7.3	NC	WB	1021	8.7
WB	WB	845	7.2	WB	WB	327	2.8
WB	NZ	211	1.8	O	WB	316	2.7
(C) within bankfull normal channel				(H) hosting bankfull normal channel			
NC	NC	4750	40.4	NC	NC	2759	23.5
NC	WB	1001	8.5	WB	NC	1350	11.5
NC	CP	772	6.6	CP	NC	1258	10.7
(D) within bankfull constricted pool				(I) hosting bankfull constricted pool			
CP	NC	1305	11.1	NC	CP	853	7.3
CP	CP	1008	8.6	CP	CP	841	7.2
CP	O	99	0.8	NZ	CP	345	2.9
(E) within bankfull oversized				(J) hosting bankfull oversized			
O	NC	50	0.4	NC	O	31	0.3
O	O	15	0.1	O	O	26	0.2
O	WB	7	0.1	WB	O	16	0.1

*O=oversized, CP=constricted pool, NC=normal channel, WB=wide bar, NZ=nozzle (positive, high Zs) base flow units (Figure 10a,b), meaning that both the bankfull and base flow features were likely formed at the same time, and thus driven by higher flood mechanisms, not by bankfull flow mechanisms. Similarly, bankfull constricted pool units had deep units nested within them (Figures 9 and 10), also suggesting that they were formed together at higher flow through scour mechanisms. Oversized had both oversized and wide bar nested within, so that means that they were formed conditionally on what higher flow units were doing.

In light of the indications that both bankfull and base flow units were likely formed at the same time, an analysis was done to see what each bankfull unit type was nested within at the floodprone flow (Table 7f-j). For every bankfull landform, the case where that landform type is nested into the same type at the floodprone scale was in the top two most frequent permutations. This outcome is illustrated by the several of the units shown in Figure 10 and is a strong indication that bankfull landforms are locked in to the same unit type at the next scale up, which means that the next scale up controls them, or both scales are controlled by an even larger scale dynamic. Bankfull wide bar occurred predominantly in normal channel floodprone landforms and secondarily over floodprone wide bar, but also in oversized floodprone landforms. The section shown in Figure 9 illustrates these nesting scenarios. Bankfull wide bars are thought to be depositional features, and thus it makes sense that they are preferentially nested in places with low to average velocity at higher discharges. Yet, that means that the common interpretation of a simple two-stage riffle-pool self-maintenance mechanism may in fact be influenced by or completely dominated by flow convergence routing and sediment deposition on wide bars during much larger floods > $8 \cdot Q_{bf}$. Conversely, bankfull constricted pool occurred in floodprone landforms that had high velocity, which were constricted pool and secondarily nozzle, as well as in normal channel floodprone landforms. Bankfull normal channel was primarily hosted in normal channel floodprone landforms as well as wide bar and constricted pool floodprone landforms. They were most rare in floodprone nozzles. Oversized bankfull landforms occurred in normal channel and oversized floodprone landforms most, and then wide bar floodprone landforms.

Bankfull nozzle occurred in nearly equal occurrence in normal and nozzle floodprone landforms, and then secondarily in wide bar ones. This result means that nozzle was uniformly present over all three spatial scales as one major type for nozzle (Figure 10), and these appear to be locations with highly resistant beds or channel dimensions tightly constrained by human intervention at all scales, otherwise how could they persist against the highest velocities present along the river. Bankfull nozzles nested within wide bar floodprone landforms suggest a bar-chute morphology in which sediment deposited during a large flood is then dissected with chutes to form bankfull flow pathways, likely on the falling limb of the flood. This result is similar to the finding of bankfull wide bars hosting base flow nozzles, again suggesting a smaller scale type of bar-chute complex in such locations.

Discussion

Traditionally, geomorphologists viewed riffle-pool self-maintenance as largely due to a relocation in peak velocity from over riffles at low flow to over pools during high flow

(Keller, 1971). Subsequent work generalized the driving force from velocity to shear stress and Shields stress to account for bed material differences (Cao *et al.*, 2003; Jackson *et al.*, 2015), but this retained the fundamental two-stage conceptualization in which material eroded out of pools (and that transported from upstream) deposits on riffles. Milan *et al.* (2001) reported that shear stress reversals may occur at different river stages during a flood hydrograph for up to just over Q_{bf}, while Sawyer *et al.* (2010) reported multiple velocity reversals during a flood of $7.63 \cdot Q_{bf}$ at one pool-riffle-run sequence.

This study looks at the widest flow range to date and with many novel tests. It also used a highly dynamic river undergoing significant erosion and deposition as its testbed (Carley et al, 2012). Study results call the classic two-stage mechanism into question. Specifically, on the lower Yuba River, results show that in-channel and bankfull channel morphologies are not just controlled by flows at those scales, but to a large degree are set by morphodynamics induced by floods interacting with multiple scales of topographic heterogeneity within the floodprone area. This conclusion is not unprecedented. Sawyer *et al.* (2010) was the first to look across a modest range of flood flows and find a three-stage shift in the location of peak velocity. Most recently, Strom *et al.* (2016) showed that flow convergence routing occurs with a diversity of hydraulic patch behaviors across many flows and that each type of morphological unit exhibits a unique velocity versus discharge relation. The extent to which these results apply elsewhere will require more studies of hierarchical landform nesting to find out.

Hierarchical topographic complexity

This study looked at an alluvial river in its transition from the foothills to the wide valley floor and found wide variations in detrended bed elevation and width. Further, those variations were largely organized, with high Zs and Ws coinciding and low Zs and Ws coinciding. That means that the river is primarily organized into wide bars alternating with constricted pools at flows from zero to $2 \cdot Q_{bf}$, and thus two-stage flow convergence routing is most likely to be present.

Yet the structure of topographic complexity does not end at the channel banks. Wide swings in Ws and Zs were found at all flows. For moderate to large floods, these higher frequency variations were on top of large coherent constrictions and expansions stemming from natural and anthropogenic constraints on valley floor morphology. That means that width is adjustable to a degree, but that forced width constraints drive more adjustments in Zs than Ws.

Velocity patterns confirmed

To a large degree, 2D modeling of river velocity corroborated the morphodynamic theory underlying the landform classification proposed and implemented in this study. That is important, because it means that people can move forward with assessing the functionality of flow convergence routing in their rivers based on topographic analysis of a meter-resolution DEM, without having to do 2D modeling. Even though 2D modeling is gaining popularity and is useful when assessing river conditions and test river engineering designs (Pasternack and Brown, 2013), mechanistic tools are needed for river analysis at the project planning stage, long before designs are ready for 2D modeling. The framework used in this study only requires a DEM (Gore and Pasternack, 2016).

Still, rivers exhibit complex lateral velocity fields, especially during floods, and thus nozzles may not have the highest velocity and oversized the lowest (Figures 6 and 7). First, the landform classification is based on thresholds and therefore does not consider exact cross-sectional areas. To be classified as a nozzle in this system, all that has to happen is that a cross section's absolute value of Ws·Zs has to be greater than 0.5 and the cross section has to be narrower and shallower than average. However, it is plausible that a constricted pool might be deeper than average, but so disproportionately narrow that its cross section is smaller than that of a nozzle. This geometry is exactly what happened at the site shown in Figure 7c. Similarly, a wide bar might be shallower than average, yet its cross-section is so vast that its cross-sectional area is greater than that of oversized. In these cases, even if velocity had a uniform distribution across the water surface area, nozzle would not be fastest and oversized would not be slowest.

Second, rivers exhibit strong lateral variation in velocity in response to topographic complexity. Abrupt expansions and constrictions can cause hydraulic jetting with a narrow effective width conveying most flow flanked by one or two peripheral recirculations (Thompson *et al.*, 1996; Clifford, 1993). Alternately, a river may exhibit large, laterally discrete inundation zones with significantly different depths and velocities during floods, and thus a cross-sectional average interpretation may not fit well.

Finally, this classification does not account for landform differences in bed and water surface slopes that drive differences in landform-stratified velocity. At the reach scale, LYR has a relatively narrow slope range. However, at the landform scale it is possible that there are significant differences that have been neglected. This geometry is unlikely in this study because constricted pools are definitely not steeper sloped than nozzles, but it is easily imaginable for a mountain river segment. Yet even then, the purpose of the method in this study was to isolate an individual process, in this case the process associated with variations in width and depth that drive flow convergence routing. Slope patterns could be captured with a second functional classification and then merged with this one, as envisioned in the conceptualization in the study purpose section.

Nesting reveals new understanding

Among the diverse results in this study, one particularly novel outcome is that the focus on the structure of topographic heterogeneity revealed that base flow and bankfull channel landforms are in fact organized together as dictated by the topographic steering of the landforms at the floodprone scale (Table 7). Specifically, bankfull wide bars and constricted pools are preferentially nested in floodprone wide bars and constricted pools, respectively. The expansion or constriction of the floodprone region controls erosion and deposition of the bankfull channel during modest floods. It is also important that during in-channel and bankfull flows on the LYR, 2D modeling predicts that gravel and cobble substrates are largely immobile (except at knickpoints), so the notion that a two-stage self-maintenance mechanism can be in play is refuted in this case. These model findings are consistent with our extensive field observations of the river during such flows over the last 15 years. Some lateral migration of locally over-steepened, noncohesive banks has been observed in TBR at bankfull or lower flows, but the volumes are comparatively small. For other rivers with much smaller substrate sizes and significantly higher Shields stresses, a two-stage mechanism may be plausible. Nevertheless, on the LYR base flow and bankfull channel geometries, especially their structured nonunifomity, are set during floods. Recent topographic change detection and analysis studies (Wyrick and Pasternack, 2015; Pasternack and Wyrick, 2016) showed that during the epoch from 1999 to 2008, a series of high-magnitude, long-duration floods, including one instantaneous peak of ~ 23 times bankfull discharge, drove rejuvenation of the diversity of in-channel morphological units at the subwidth spatial scale. Overall, multiple studies looking at hydraulics, topographic structure, and morphodynamics now provide a coherent conceptualization of the importance of hierarchical topographic structure in controlling how the LYR functions.

Conclusions

This study answered 16 scientific questions organized under four objectives. At the highest level this study showed that it is possible to analyze the hierarchical nesting of landforms in a data-rich setting to provide a scale-independent typology that yields a unified conceptualization of morphodynamics over a wide range of scales. Given that capability, this study found that base flow and bankfull channel landforms are most likely structured not by their own flow-dependent interactions, but by an overarching role for valley-scale topographic steering of large floods that occur roughly every decade or less frequently. This finding has important implications for professional practices in river management and engineering, because practitioners must now look beyond the bankfull channel to obtain self-sustainable riverine landforms within the channel.

Acknowledgements

Precursor data were collected for different purposes with funding from the Yuba County Water Agency (Award #201016094) and as in-kind aid from the Yuba Accord River Management Team. Time spent processing and analyzing data was funded by Yuba County Water Agency (Award #201016094). This project was also supported by the USDA National Institute of Food and Agriculture, Hatch project number #CA-D-LAW-7034-H. We thank Dr. Roser Casas-Mulet, Joni Gore, Belize Lane, Dr. Michael Stewardson, Anne Senter, and Jason Wiener for constructive reviews of a draft of this manuscript prior to journal submission as well as Dr. Stuart Lane and anonymous reviewers for constructive guidance in manuscript revision.

References

Abu-Aly TR, Pasternack GB, Wyrick JR, Barker R, Massa DA, Johnson TR. 2014. Effects of LiDAR-derived, spatially distributed vegetation roughness on two-dimensional hydraulics in a gravel-cobble river at flows of 0.2 to 20 times bankfull. Geomorphology **206**: 468-482. DOI: 10.1016/j.geomorph.2013.10.017.

Angermeier PL, Smogor RA. 1995. Estimating number of species and relative abundances in stream-fish communities: effects of sampling effort and discontinuous spatial distributions. Canadian Journal of Fisheries and Aquatic Sciences **52**: 936-949. DOI: 10.1139/f95-093.

Barenblatt GI, Monin AS. 1979. Similarity laws for turbulent stratified shear flows Archive for Rational Mechanics and Analysis **70**: 307. DOI:10.1007/BF00281157.

Barker JR. 2011. Rapid, abundant velocity observation to validate million-element 2D hydrodynamic models. MS Thesis, University of California at Davis: Davis, CA.

Beechie TJ, Sear DA, Olden JD, Pess GR, Buffington JM, Moir H, Roni P, Pollock MM. 2010. Process-based Principles for Restoring River Ecosystems. Bioscience **60**: 209-222. DOI: 10.1525/bio.2010.60.3.7

Brasington J, Vericat D, Rychkov I. 2012. Modeling river bed morphology, roughness, and surface sedimentology using high resolution terrestrial laser scanning. Water Resources Research **48**: W11519, doi:10.1029/2012WR012223.

Brennan JM, Bender DJ, Contreras TA, Fahrig L. 2002. Focal patch landscape studies for wildlife management: optimizing sampling effort across scales. In *Integrating Landscape Ecology Into Natural Resource Management*, Liu J, Taylor WW (eds). Cambridge University Press: New York, NY; 68-91.

Brierley GJ, Fryirs K. 2000. River styles, a geomorphic approach to catchment characterization: Implications for river rehabilitation in Bega catchment, New South Wales, Australia. Environmental Management **25**: 661-679.

Brown RA, Pasternack GB. 2014. Hydrologic and topographic variability modulate channel change in mountain rivers. Journal of Hydrology **510**: 551-564. DOI: 10.1016/j.jhydrol.2013.12.048.

Brown RA, Pasternack GB. 2017. Bed and width oscillations form coherent patterns in a partially confined, regulated gravel–cobble-bedded river adjusting to anthropogenic disturbances. Earth Surf. Dynam. **5**: 1-20. DOI: 10.5194/esurf-5-1-2017.

Brown RA, Pasternack GB, Wallender WW. 2014. Synthetic river valleys: Creating prescribed topography for form–process inquiry and river rehabilitation design. Geomorphology **214**: 40-55. DOI: 10.1016/j.geomorph.2014.02.025

Cao ZX, Carling P, Oakey R. 2003. Flow reversal over a natural pool-riffle sequence: A computational study. Earth Surface Processes and Landforms **28**: 689-705.

Carley JK, Pasternack GB, Wyrick JR, Barker JR, Bratovich PM, Massa DA, Reedy GD, Johnson TR. 2012. Significant decadal channel change 58-67 years post-dam accounting for uncertainty in topographic change detection between contour maps and point cloud models. . Geomorphology **179**: 71-88. DOI: doi:10.1016/j.geomorph.2012.08.001.

Clifford NJ. 1993. Formation of riffle-pool sequences: Field evidence for an autogenetic process, Sedimentary Geology **85**: 39-51.

Frissell CA, Liss WJ, Warren CE, Hurley MD. 1986. A hierarchical framework for stream habitat classification: Viewing streams in a watershed context. Environmental Management **10**: 199-214. DOI: 10.1007/bf01867358.

Gilbert GK. 1917. *Hydraulic-mining Debris in the Sierra Nevada*, US Geological Survey Professional Paper 105, US Geological Survey, Washington, DC.

Gonzalez RL, Pasternack GB. 2015. Reenvisioning cross-sectional at-a-station hydraulic geometry as spatially explicit hydraulic topography. Geomorphology **246**: 394-406. DOI: 10.1016/j.geomorph.2015.06.024

Gore J, Pasternack GB. 2016. Analysis and classification of topographic flow steering and inferred geomorphic processes as a function of discharge in a mountain river. Abstract EP53D-1016 presented at 2016 Fall Meeting, AGU, San Francisco, Calif., 12-16 Dec.

Hay GJ, Marceau DJ, Dubé P, Bouchard A. 2001. A multiscale framework for landscape analysis: Object-specific analysis and upscaling. Landscape Ecology **16**: 471-490. DOI: 10.1023/a:1013101931793.

Horton RE. 1945. Erosional Development Of Streams And Their Drainage Basins; Hydrophysical Approach To Quantitative Morphology. Geological Society of America Bulletin **56**: 275-370. DOI: 10.1130/0016-7606(1945)56[275:edosat]2.0.co;2

Hunsaker CT, Levine DA. 1995. Hierarchical Approaches to the Study of Water Quality in Rivers. Bioscience **45**: 193-203. DOI: 10.2307/1312558.

Imhol JG, Fitzgibbon J, Annable WK. 1996. A hierarchical evaluation system for characterizing watershed ecosystems for fish habitat. Canadian Journal of Fisheries and Aquatic Sciences **53**: 312-326. DOI: 10.1139/f96-011

Jackson JR, Pasternack GB, Wheaton JM. 2015. Virtual manipulation of topography to test potential pool–riffle maintenance mechanisms. Geomorphology **228**: 617-627. DOI: 10.1016/j.geomorph.2014.10.016.

Jakubauskas ME, Legates DR, Kastens JH. 2002. Crop identification using harmonic analysis of time-series AVHRR NDVI data. Computers and Electronics in Agriculture **37**: 127-139. DOI: http://dx.doi.org/10.1016/S0168-1699(02)00116-3.

Keller EA. 1971. Areal Sorting of Bed-Load Material - Hypothesis of Velocity Reversal. Geological Society of America Bulletin **82**: 753-756.

Kumar P, Foufoula-Georgiou, E. 1997. Wavelet analysis for geophysical applications. Reviews of Geophysics **35**: 385-412. doi:10.1029/97RG00427.

Legleiter CJ. 2014. A geostatistical framework for quantifying the reach-scale morphology: 1. Variogram models, related metrics, spatial structure of river and relation to channel form. Geomorphology **205**: 65-84.

Legleiter CJ, Roberts DA, Lawrence RL. 2009. Spectrally based remote sensing of river bathymetry. Earth Surface Processes and Landforms **34**: 1039-1059.

Mandlburger G, Hauer C, Wieser M, Pfeifer N. 2015. Topo-Bathymetric LiDAR for Monitoring River Morphodynamics and Instream Habitats—A Case Study at the Pielach River. Remote Sensing **7**: 6160.

Milan DJ, Heritage GL, Large ARG, Charlton ME. 2001. Stage dependent variability in tractive force distribution through a riffle-pool sequence. Catena **44**: 85-109.

Neeson TM, Gorman AM, Whiting PJ, Koonce JF. 2008. Factors Affecting Accuracy of Stream Channel Slope Estimates Derived from Geographical Information Systems. North American Journal of Fisheries Management **28**: 722-732.

Pasternack GB. 2011. *2D Modeling and Ecohydraulic Analysis*. Createspace, Seattle, WA.

Pasternack GB, Brown RA. 2013. Ecohydraulic design of riffle-pool relief and morphological-unit geometry in support of regulated gravel-bed river rehabilitation. In *Ecohydraulics: an integrated approach*, Maddock I, Harby A, Kemp P, Wood PJ (eds). John Wiley & Sons, Ltd.: Chichester, UK; 337-355.

Pasternack GB, Brown RA. 2016. Designing rivers with multiple scales of channel and floodplain variation to yield diverse processes and ecosystem services. In *11th International Conference on Ecohydraulics*. International Association for Hydro-Environment Engineering and Research: Melbourne, Australia; 1-4.

Pasternack GB, Wyrick JR. 2016. Flood-driven topographic changes in a gravel-cobble river over segment, reach, and morphological unit scales. Earth Surface Processes and Landforms **42**: 487-502. DOI: 10.1002/esp.4064.

Pasternack GB, Tu D, Wyrick JR. 2014. Chinook adult spawning physical habitat of the lower Yuba River. Prepared for the Yuba Accord River Management Team. University of California: Davis, CA.

Pasternack GB, Baig D, Webber M, Brown, R. 2018. Hierarchically nested river landform sequences. Part 1: Theory. Earth Surface Processes and Landforms. DOI: 10.1002/esp.4411.

Pawlowicz R, Beardsley B, Lentz S. 2002. Classical tidal harmonic analysis including error estimates in MATLAB using T_TIDE. Computers & Geosciences **28**: 929-937. DOI: http://dx.doi.org/10.1016/S0098-3004(02)00013-4.

Priestley MB. 1981. *Spectral Analysis and Time Series*. Academic Press: London.

Rodriguez-Iturbe I, Rinaldo A. 1997. *Fractal River Basins- Chance and Self-Organization*. Cambridge University Press: New York, NY.

Rosgen DL. 1994. A Classification of Natural Rivers. Catena 22: 169-199.

Sawyer AM, Pasternack GB, Moir HJ, Fulton AA. 2010. Riffle-pool maintenance and flow convergence routing observed on a large gravel-bed river. Geomorphology **114**: 143-160. DOI: 10.1016/j.geomorph.2009.06.021.

Smith KL, Jones ML. 2008. Allocation of Sampling Effort to Optimize Efficiency of Watershed-Level Ichthyofaunal Inventories. Transactions of the American Fisheries Society **137**: 1500-1506. DOI: 10.1577/T07-024.1

Strom MA, Pasternack GB, Wyrick JR. 2016. Reenvisioning velocity reversal as a diversity of hydraulic patch behaviours. Hydrological Processes **30**: 2348-2365. DOI: 10.1002/hyp.10797.

Thompson DM, Wohl EE, Jarrett RD. 1996. A revised velocity reversal and sediment sorting model for a high-gradient, pool-riffle stream, Physical Geography **17**: 142-156.

Thomson JR, Taylor MP, Brierley GJ. 2004. Are River Styles ecologically meaningful? A test of the ecological significance of a geomorphic river characterization scheme. Aquatic Conservation-Marine and Freshwater Ecosystems **14**: 25-48.

Thomson JR, Taylor MP, Fryirs KA, Brierley GJ. 2001. A geomorphological framework for river characterization and habitat assessment. Aquatic Conservation-Marine and Freshwater Ecosystems **11**: 373-389.

Westoby MJ, Brasington J, Glasser NF, Hambrey MJ, Reynolds JM. 2012. 'Structure-from-Motion' photogrammetry: A low-cost, effective tool for geoscience applications. Geomorphology **179**: 300-314. DOI: http://dx.doi.org/10.1016/j.geomorph.2012.08.021

Woldenberg MJ. 1969. Spatial Order in Fluvial Systems: Horton's Laws Derived from Mixed Hexagonal Hierarchies of Drainage Basin Areas. Geological Society of America Bulletin 80: 97-112. DOI: 10.1130/0016-7606(1969)80[97:soifsh]2.0.co;2

Wyrick JR, Pasternack GB. 2012. Landforms of the Lower Yuba River. Prepared for the Yuba Accord River Management Team. University of California at Davis: Davis, CA.

Wyrick JR, Pasternack GB. 2014. Geospatial organization of fluvial landforms in a gravel-cobble river: beyond the riffle-pool couplet. . Geomorphology **213**: 48-65. DOI: doi:10.1016/j.geomorph.2013.12.040.

Wyrick JR, Pasternack GB. 2015. Revealing the natural complexity of topographic change processes through repeat surveys and decision-tree classification. Earth Surface Processes and Landforms **41**: 723-737. DOI: 10.1002/esp.3854.

Table Captions

Table 1. Scientific analysis framework for this study applied to whole river segment and each geomorphic reach.

Table 2. Metrics for topographic variability. Dark and light shading indicate highest and lowest values, respectively.

Table 3. Results of Ws·Zs analysis. Dark and light shading indicate highest and lowest values, respectively.

Table 4. Analysis of landform composition as a function of flow.

Table 5. Longitudinal sequencing of landforms for the whole river, excluding normal channel units.

Table 6. Top five permutations of hierarchical nesting of flow convergence routing landforms within the five floodprone landform types.

Table 7. Top three permutations of hierarchical nesting of bankcfull landforms, either within (A-E) or beyond (F-J) them.

Figure Captions

Figure 1. Location map of the Lower Yuba River (LYR) showing the geomorphic reaches, the key factor indicating a reach break, gaging stations, and other features of interest superimposed over the water surface area map for a flow of 1194.97 m^3/s. The reach acronyms stand for Marysville Reach (MR), Hallwood Reach (HR), Daguerre Point Dam Reach (DPDR), Dry Creek Reach (DCR), Parks Bar Reach (PBR), Timbuctoo Bend Reach (TBR), Narrows Reach (NR), and Englebright Dam Reach (EDR).

Figure 2. Longitudinal series of Zs and Ws.

Figure 3. Changes in Ws series with increasing discharge from (A) Q_{bf} to (B) $4.22 \cdot Q_{bf}$ to (C) $8.44 \cdot Q_{bf}$.

Figure 4. Pearson's product-moment correlation values for Ws and Zs, stratified by reach and flow.

Figure 5. Series of Ws·Zs for three flows with colors representing landform type.

Figure 6. Landform-stratified 2D-model velocity results, (A) mean and (B) 95th percentile.

Figure 7. Examples illustrating (A) simple and (B), (C) complex velocity patterns at the indicated flows.

Figure 8. Idealized two-level nested channel illustrating a typical nesting scenario.

Figure 9. Sample map showing the scale-independent landforms at a location where (A) base flow nozzles (N, red patches) are nested within (B) bankfull wide bar units (WB, orange patches), which in turn are nested within bankfull oversized (O, black patches) and mixed normal channel-wide bar units (NC/WB, grey-orange patches). Flow is from right to left.

Figure 10. Sample map showing the scale-independent landforms at a location where (A) base flow nozzles are nested within (B) bankfull nozzles, but the bankfull nozzles are nested in (C) three different floodprone landforms- constricted pool, nozzle, and normal channel. Legend is the same as the previous figure. Flow is from right to left.

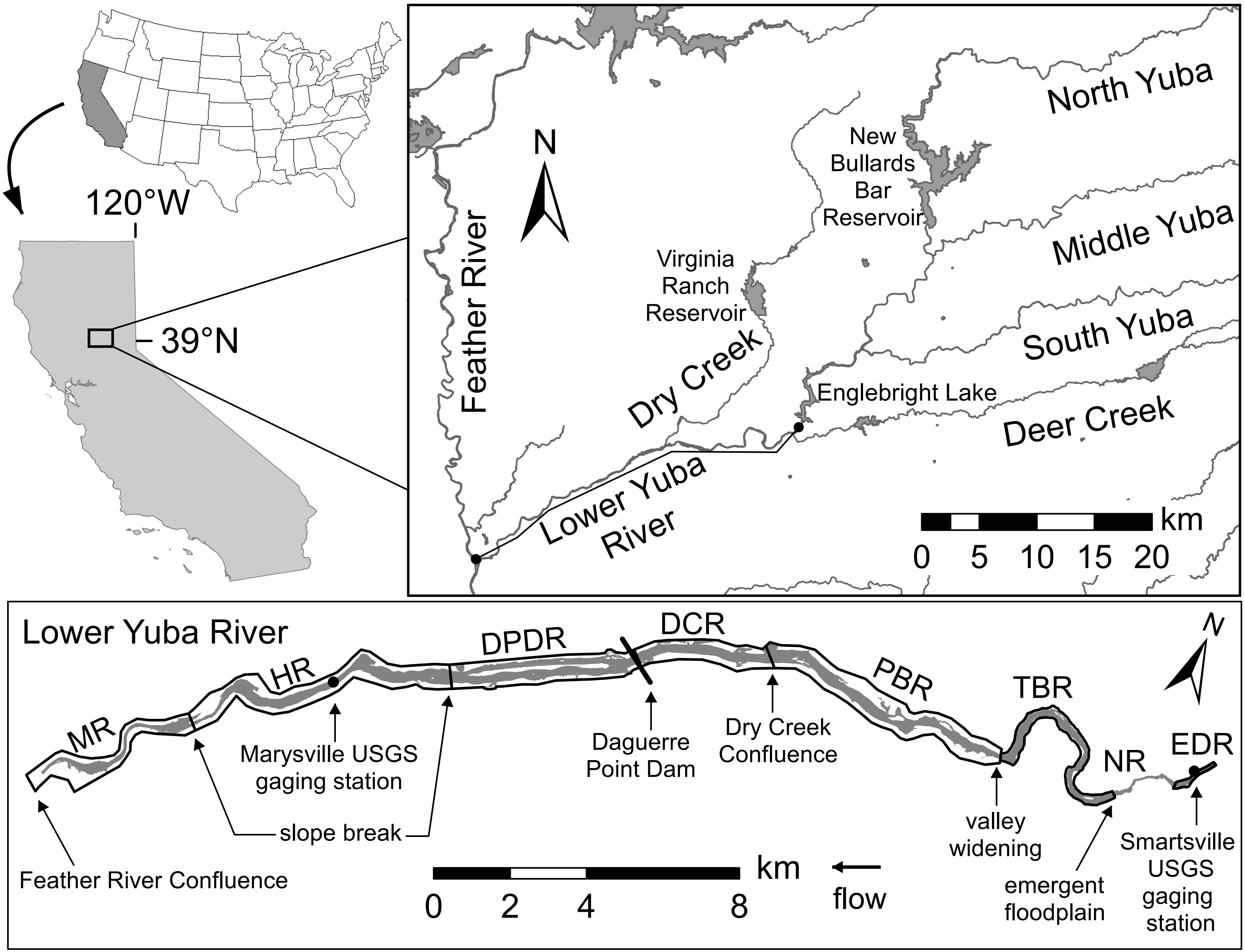
120°W
39°N
N
Feather River
Dry Creek
Virginia Ranch Reservoir
New Bullards Bar Reservoir
North Yuba
Middle Yuba
South Yuba
Deer Creek
Englebright Lake
Lower Yuba River
0 5 10 15 20 km
Lower Yuba River
MR
HR
DPDR
DCR
PBR
TBR
NR
EDR
N
Marysville USGS gaging station
slope break
Feather River Confluence
Daguerre Point Dam
Dry Creek Confluence
valley widening
emergent floodplain
Smartsville USGS gaging station
0 2 4 8 km
flow

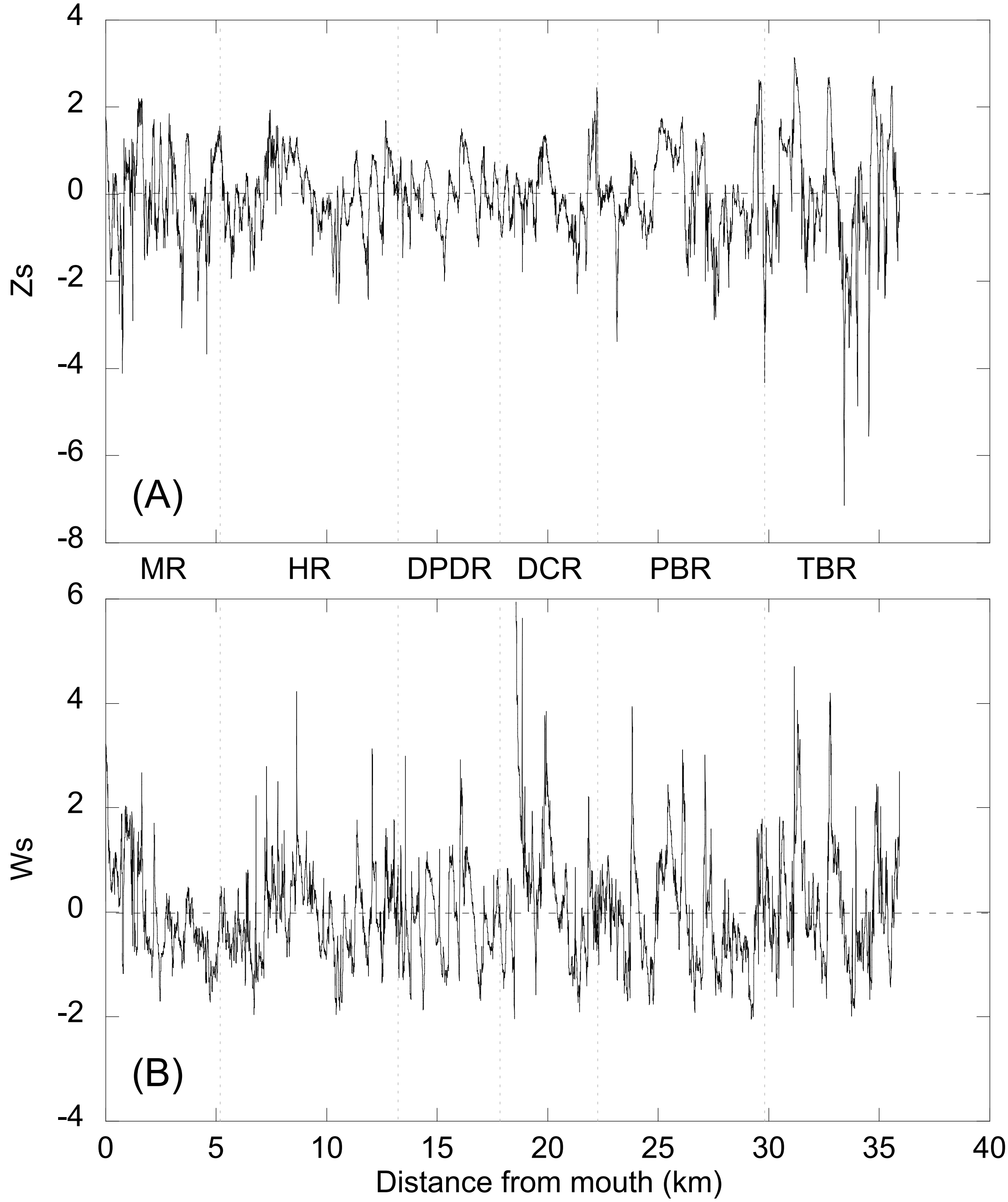

Zs
(A)
MR
HR
DPDR
DCR
PBR
TBR
Ws
(B)
Distance from mouth (km)

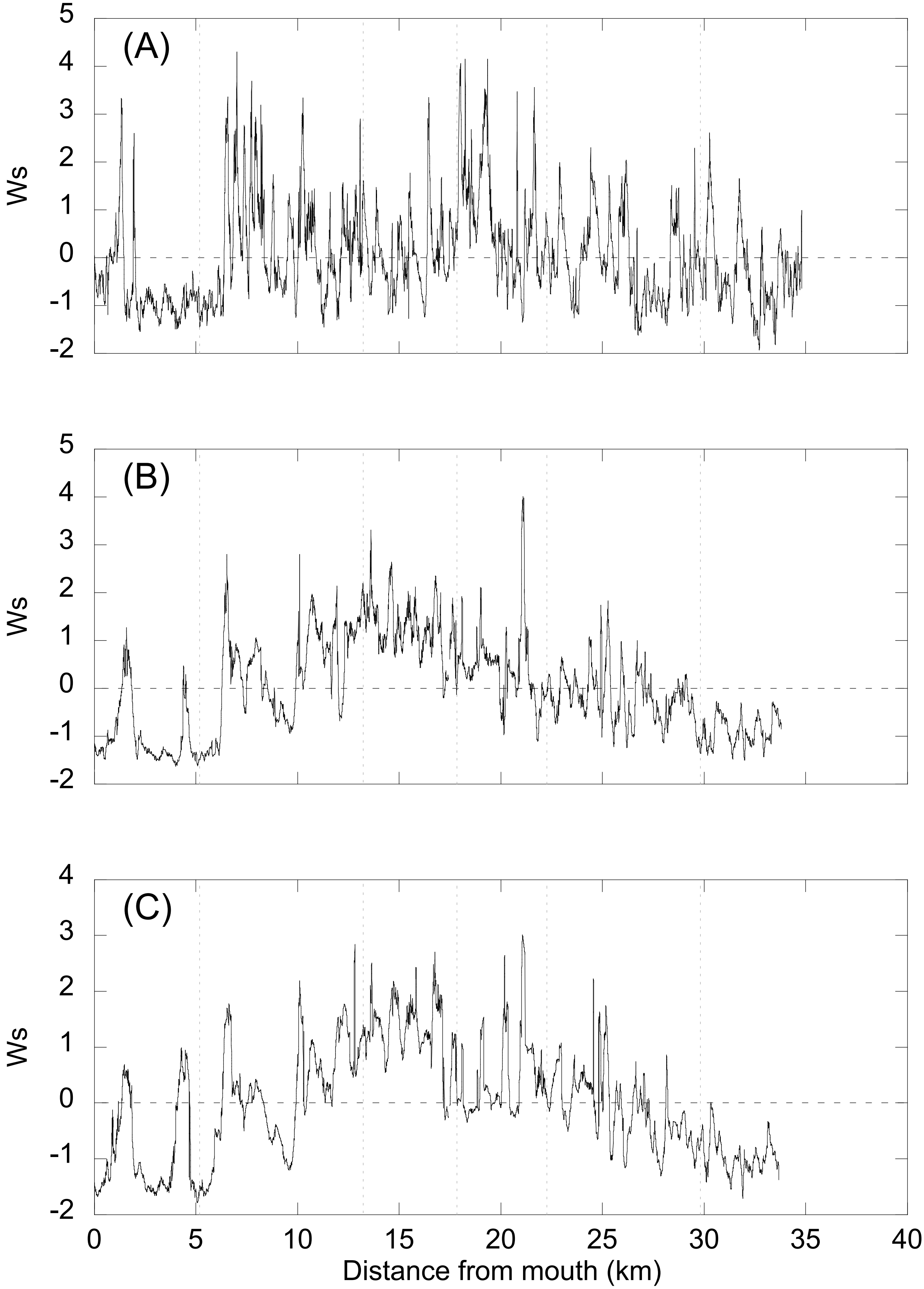
(A)
(B)
(C)
Ws
Distance from mouth (km)
5
4
3
2
1
0
-1
-2
0
5
10
15
20
25
30
35
40

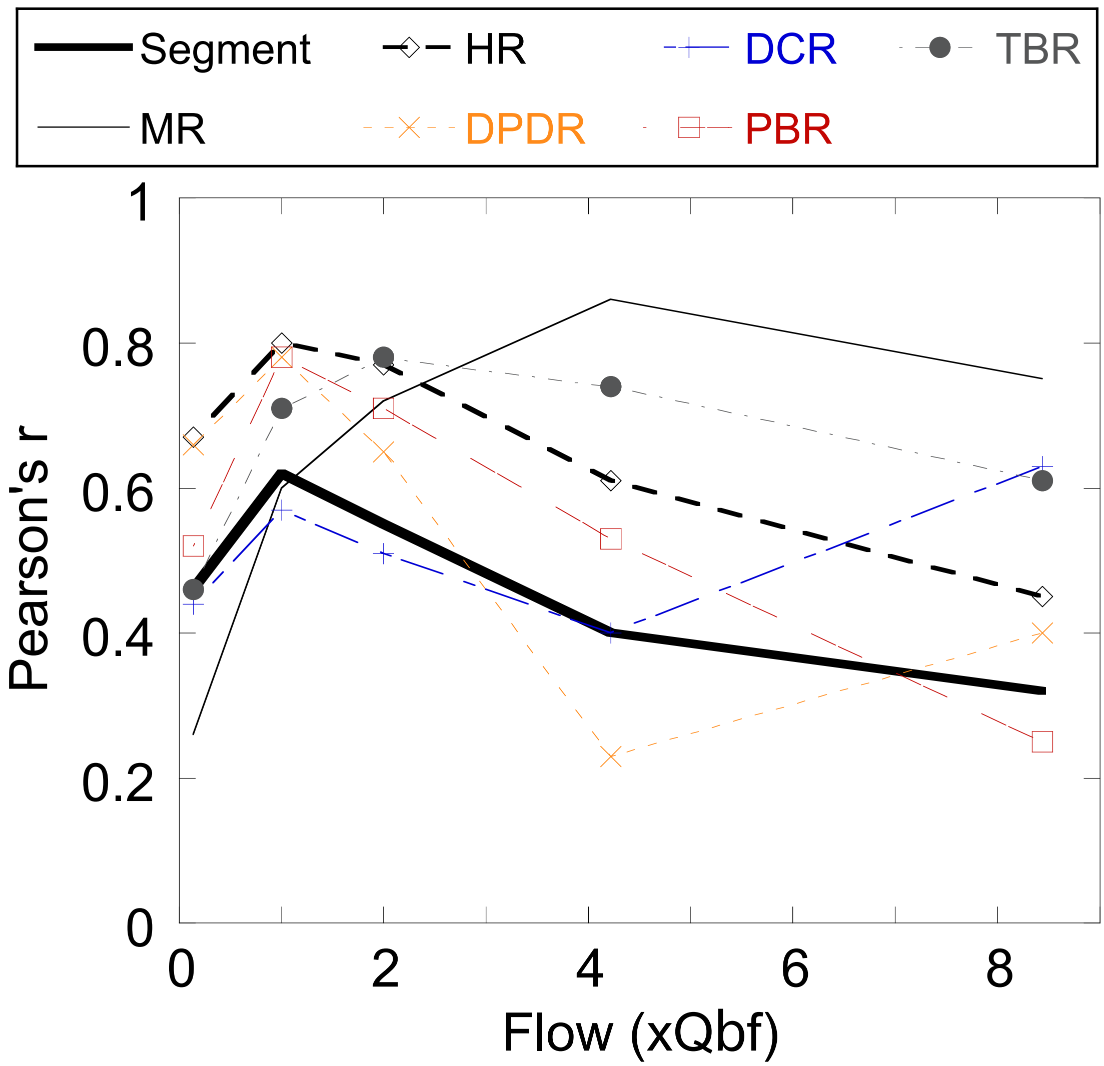

Segment
HR
DCR
TBR
MR
DPDR
PBR
Pearson's r
0
0.2
0.4
0.6
0.8
1
0
2
4
6
8
Flow (xQbf)

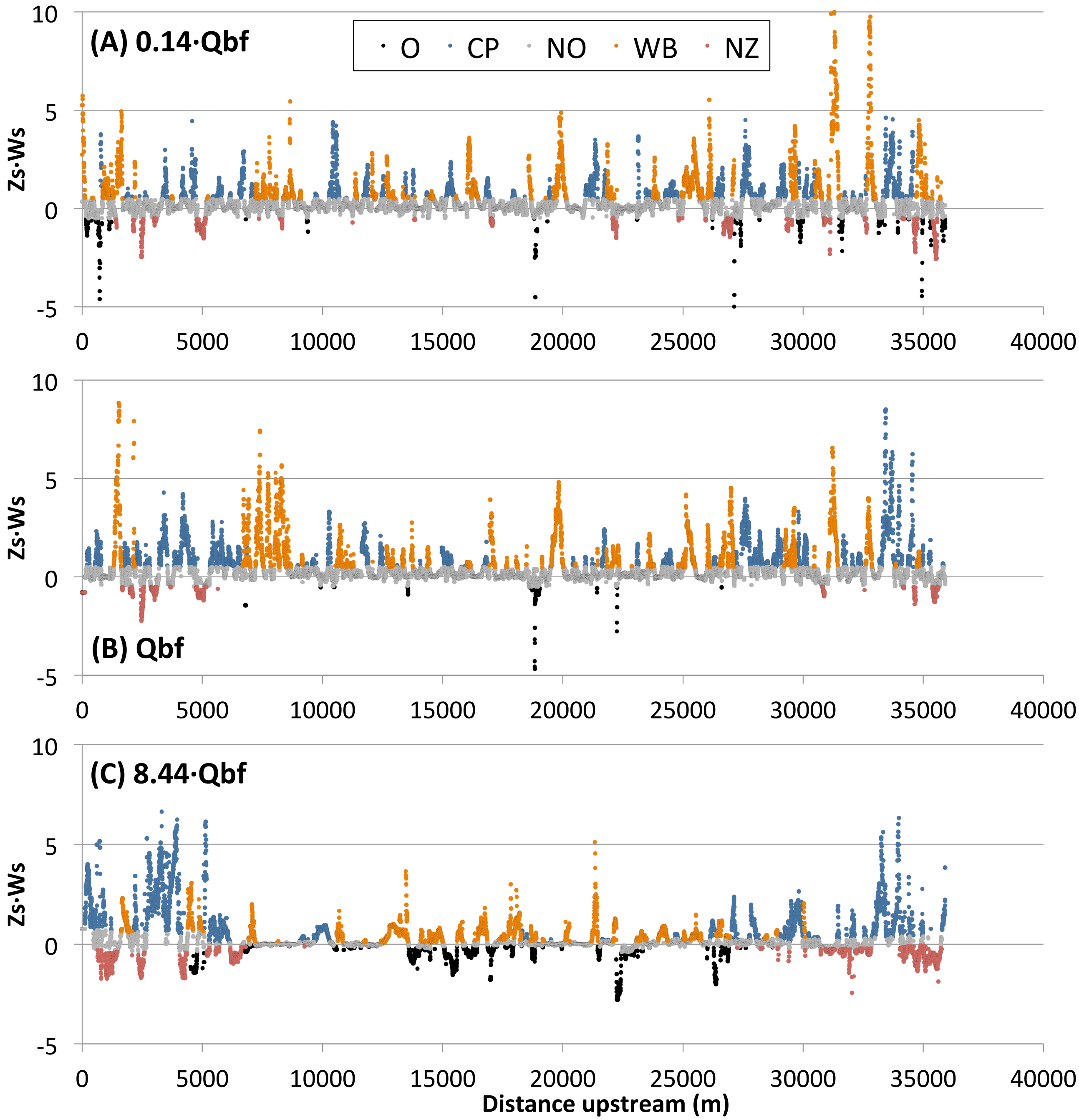

(A) 0.14·Qbf
O
CP
NO
WB
NZ
Zs·Ws
(B) Qbf
(C) 8.44·Qbf
10
5
0
-5
0
5000
10000
15000
20000
25000
30000
35000
40000
Distance upstream (m)

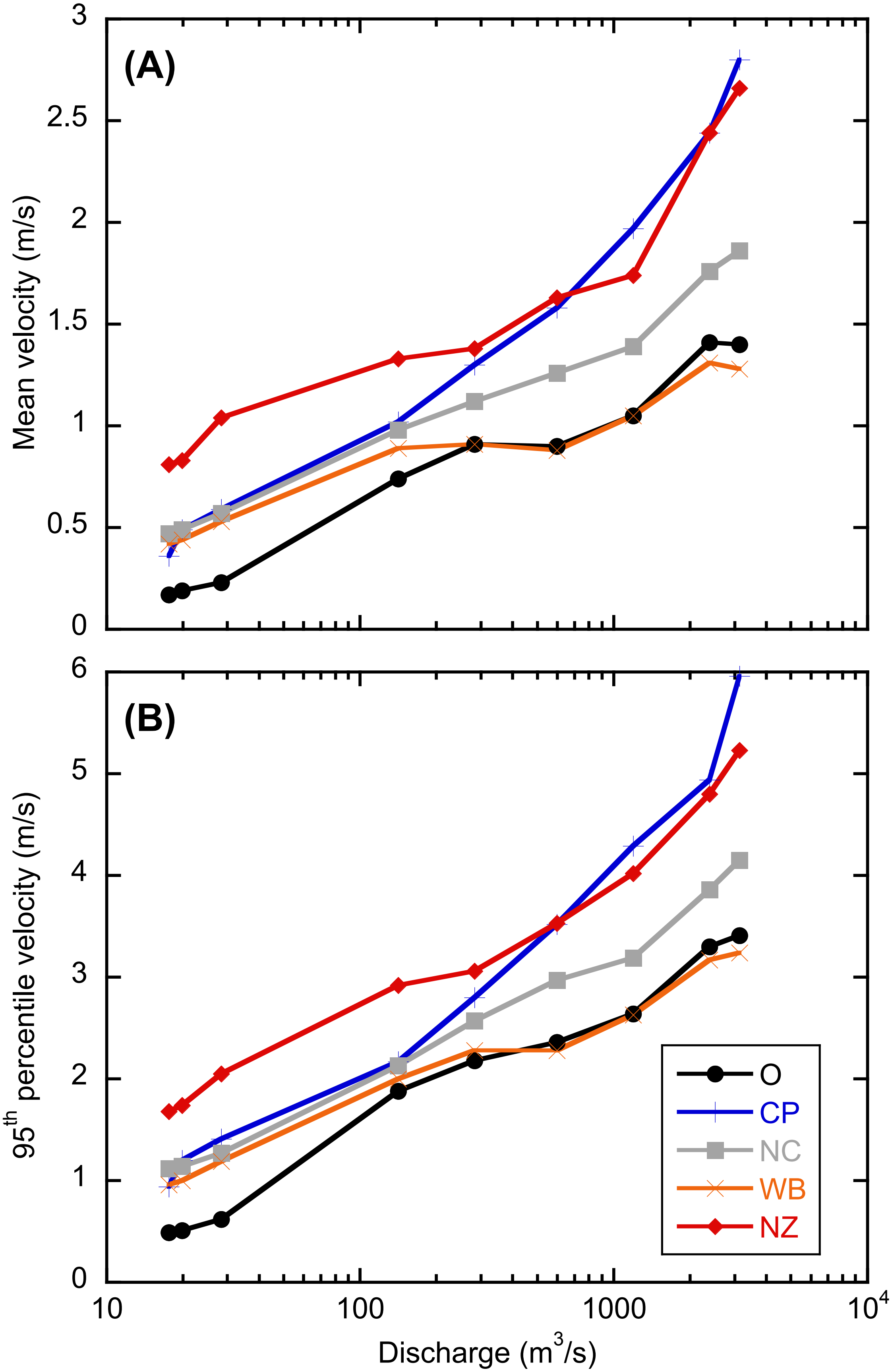

(A)
Mean velocity (m/s)
0
0.5
1
1.5
2
2.5
3
(B)
95th percentile velocity (m/s)
0
1
2
3
4
5
6
10
100
1000
10^4
Discharge (m3/s)
O
CP
NC
WB
NZ

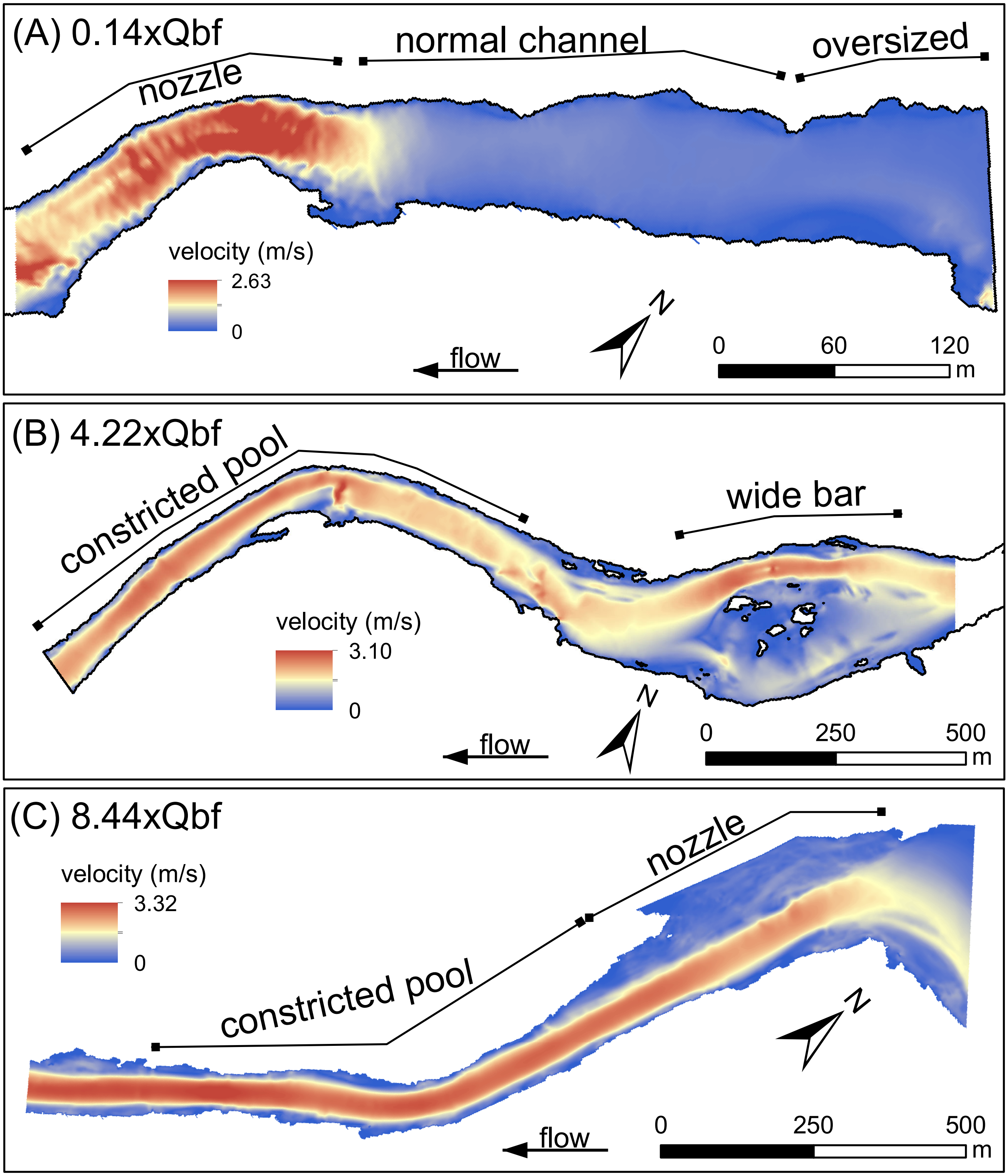
(A) 0.14xQbf
nozzle
normal channel
oversized
velocity (m/s)
2.63
0
flow
N
0
60
120
m
(B) 4.22xQbf
constricted pool
wide bar
velocity (m/s)
3.10
0
flow
N
0
250
500
m
(C) 8.44xQbf
velocity (m/s)
3.32
0
nozzle
constricted pool
N
flow
0
250
500
m

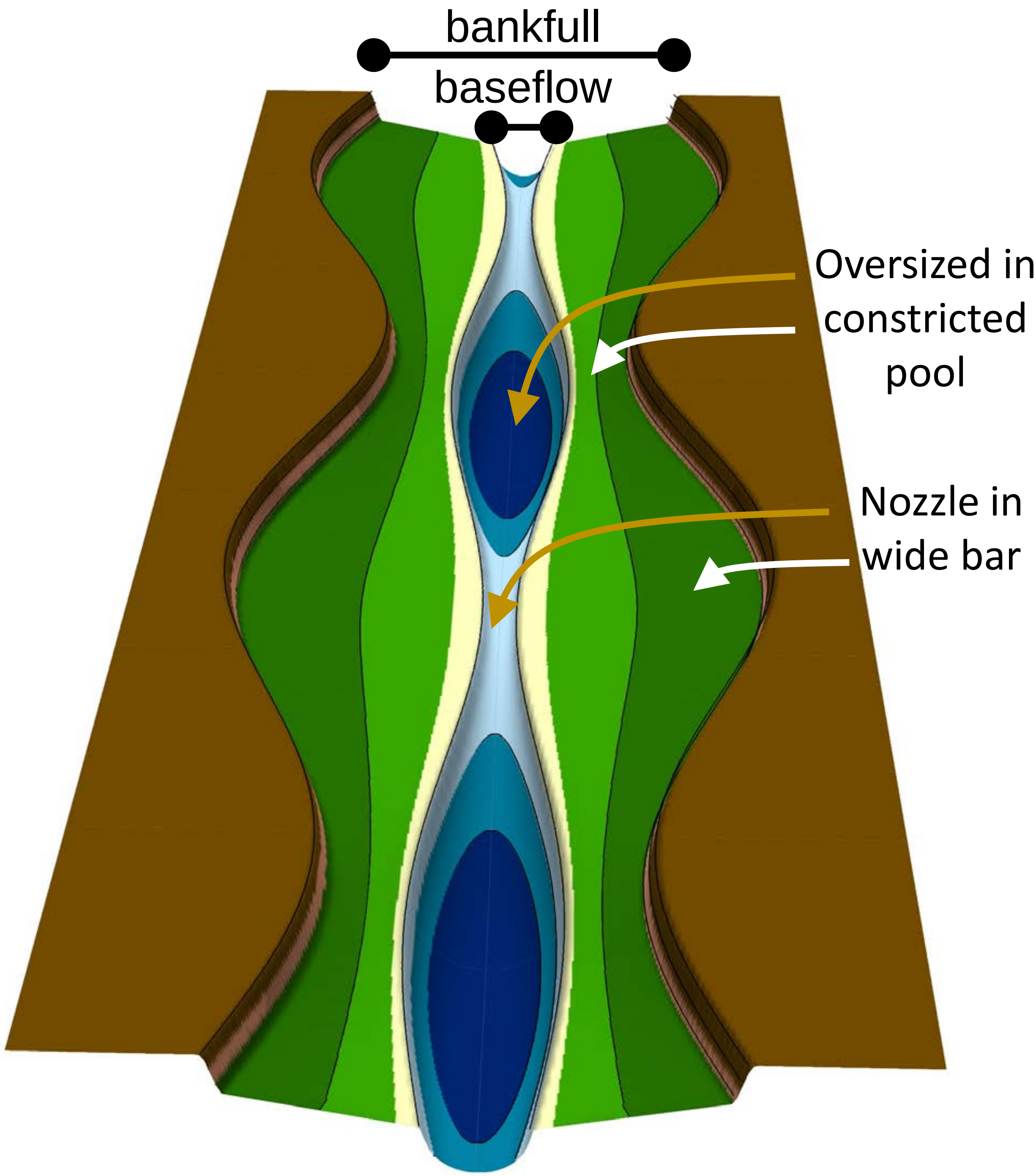
bankfull
baseflow
Oversized in
constricted
pool
Nozzle in
wide bar

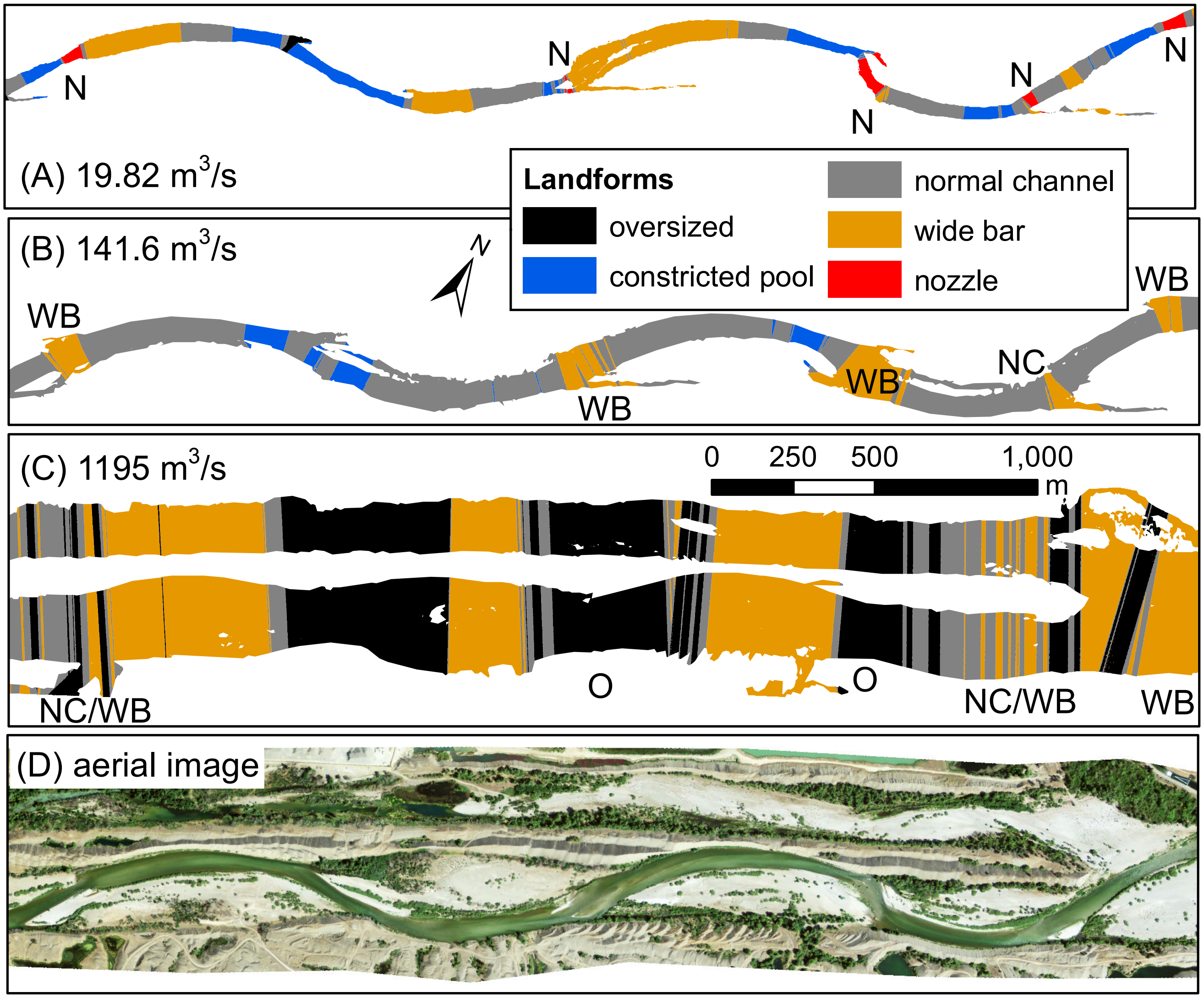

(A) 19.82 m^3/s
N
N
N
N
N
N
Landforms
oversized
constricted pool
normal channel
wide bar
nozzle
(B) 141.6 m^3/s
N
WB
WB
WB
NC
WB
(C) 1195 m^3/s
0 250 500 1,000 m
NC/WB
O
O
NC/WB
WB
(D) aerial image

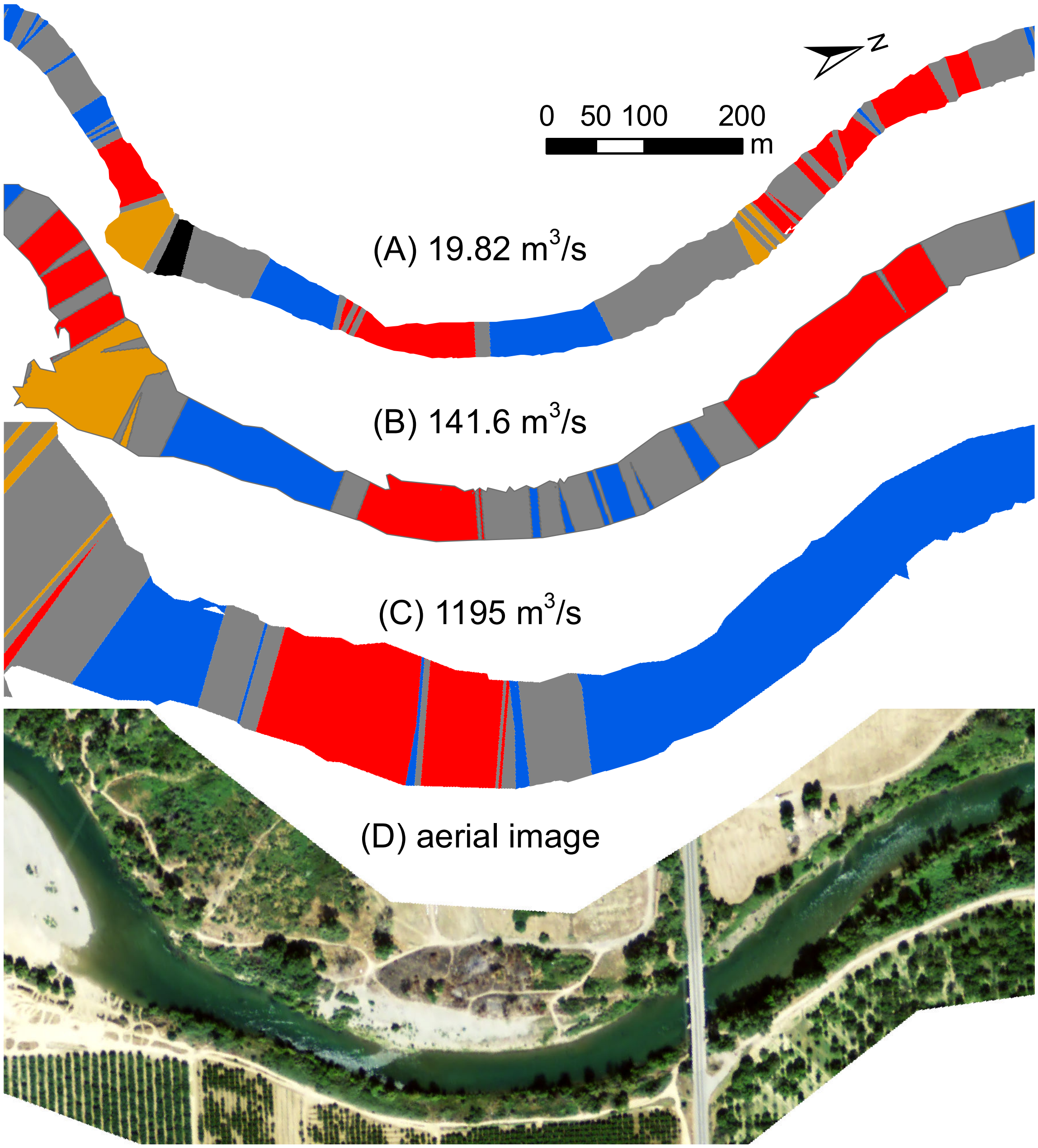

N
0 50 100 200
m
(A) 19.82 m³/s
(B) 141.6 m³/s
(C) 1195 m³/s
(D) aerial image